Ceramics International xxx (xxxx) xxx

Contents lists available at ScienceDirect

Ceramics International

journal homepage: www.elsevier.com/locate/ceramint

Synthesis and structural characterization of $CaMg_{0.5}Co_xNi_{0.5-x}Si_2O_6$ ($0 \leq x \leq 0.5$) solid solutions as a colouring substance

M.A. Tena [a,*], Mohammed S.M. Abdelbaky [b,d,**], Camino Trobajo [c], José R. García [c], Santiago Garcia-Granda [d]

[a] Inorganic Chemistry Area, Inorganic and Organic Chemistry Department, Jaume I University, P.O. Box 224, Castellón, Spain
[b] Physical Chemistry Area, Physical Chemistry Department, Salamanca University, E-37008, Salamanca, Spain
[c] Inorganic Chemistry Area, Organic and Inorganic Chemistry Department, Oviedo University-CINN, Spain
[d] Physical Chemistry Area, Physical and Analytical Chemistry Department, Oviedo University-CINN, Spain

ARTICLE INFO

Handling Editor: Dr P. Vincenzini

Keywords:
$CaMgSi_2O_6$
$CaNiSi_2O_6$
$CaCoSi_2O_6$
Diopside
Solid solutions
Pigments

ABSTRACT

In this study, $CaMg_{0.5}Co_xNi_{0.5-x}Si_2O_6$ ($0.0 \leq x \leq 0.5$) solid solutions with a diopside structure were prepared to reduce the cobalt and nickel amounts compared to M_2SiO_4 or $MgMSiO_4$ (M = Co, Ni) compounds or $CaCo_xNi_{1-x}Si_2O_6$ solid solutions. Colloidal gels were obtained by adding an ammonia aqueous solution to the suspensions of precursors in aqua until pH = 10. Diopside structure began to develop at 800 °C and at 1000–1200 °C crystallinity and pink colour of materials ($x \neq 0$) are optimal. In both $CaMg_{0.5}Co_xNi_{0.5-x}Si_2O_6$ ($0.0 \leq x \leq 0.5$) and $MgCo_xNi_{1-x}SiO_4$ ($0.0 \leq x \leq 1.0$) solid solutions with diopside and olivine structures the position of the third transition of octahedral Co(II), $^4T_1 \rightarrow {}^4T_1(P)$, is centred into the green absorption range and the observed colour is pink. A higher red amount in diopside than in olivine structure can be explained by the minor width of band of this third transition (minor distortion of octahedral M1 site) and shorter mean M1-O distances (M = Ni, Co).

1. Introduction

Diopside finds technological applications in production of ceramic pigments [1]. The colour of materials with diopside structure is due to the presence of metal transition ions in their compositions. There are many advantages to synthesizing ceramic pigments using natural mineral raw materials: the calcination temperature of the pigments decreases, and raw-materials costs decrease. However, the nonuniform multiphase composition of the products is a problem for synthesis. Wollastonite, magnesium metasilicate, and forsterite are identified in addition to diopside [2]. The use of the gel method intensifies the synthesis of the crystalline diopside structure owing to a better homogenization and averaging of the batch components at the mixing stage and also because of amorphization of wollastonite. The advantages of this method include the effective formation of diopside structure at relatively low temperatures (about 1100 °C) and the mineralizing effect of the chromophores on the crystallization of these minerals [3].

$Ca(Co_xMg_{1-x})Si_2O_6$ compositions are potential pink-violet pigments [4,5]. These compositions are used in ceramic industry and synthesized from natural raw minerals to obtained unexpensive materials [2]. Using the structures of natural raw materials as the base structures, ceramic pigments with derivative crystal structures can be developed by mixing in pure oxides or other minerals. For example, the natural mineral wollastonite ($CaSiO_3$) makes possible to obtain ceramic pigments with diopside structure with the addition of MgO, SiO_2 and CoO (CoO or another chromophore oxide) and subsequent calcination at temperatures between 1100 and 1300 °C [2]. The diopside chain structure (CaO_8 and MgO_6 linked by chains of SiO_4 tetrahedrons) differs from the wollastonite chain structure (CaO_8 linked by chains of SiO_4 tetrahedrons) only by the spatial arrangement of [SiO_4^{4-}] tetrahedrons. Moreover, the presence of Mg^{2+} in the $CaO{\cdot}MgO{\cdot}2SiO_2$ composition of diopside provides for more intense incorporation of pigment ions in its lattice, since the sizes of the pigment ions (Cr^{3+}, Fe^{2+}, Fe^{3+}, Mn^{2+}, Co^{2+}, Ni^{2+}, Cu^{2+}) are close to the ionic radii of Mg^{2+} [6].

Structural information of $CaMg_{1-x}Co_xSi_2O_6$ solid solutions indicates than mean M1-O (M1 = Mg, Co) distances in C.N. = 6 are very short,

* Corresponding author.
** Corresponding author. Physical Chemistry Area, Physical Chemistry Department, Salamanca University, E-37008, Salamanca, Spain.
E-mail addresses: tena@qio.uji.es (M.A. Tena), mohammed@usal.es (M.S.M. Abdelbaky), ctf@uniovi.es (C. Trobajo), jrgm@uniovi.es (J.R. García), s.garciagranda@cinn.es (S. Garcia-Granda).

https://doi.org/10.1016/j.ceramint.2024.03.162
Received 29 October 2023; Received in revised form 20 February 2024; Accepted 12 March 2024
Available online 13 March 2024

Table 1
Unit cell and interatomic distances in $CaMSi_2O_6$ (M = Mg, Ni, Co) with diopside structure (monoclinic symmetry) and $MgMSiO_4$ (M = Mg, Ni, Co) with olivine structure (orthorhombic symmetry).

	$CaMgSi_2O_6$ (ICSD-52359)	Mg_2SiO_4 (ICSD-242067)	$CaNiSi_2O_6$ (ICSD-202244)	$MgNiSiO_4$ (ICSD-92646)	$CaCoSi_2O_6$ (ICSD-202245)	$MgCoSiO_4$ (ICSD-155359)
a(Å)	9.7300	10.1989	9.7340	10.1870	9.8060	10.3986
b(Å)	8.9100	5.9812	8.8910	5.9467	8.9500	6.0782
c(Å)	5.2500	4.7561	5.2280	4.7396	5.2430	4.8204
β(°)	105.830	90	105.870	90	105.450	90
M2-O	2.339–2.816	2.050–2.232	2.333–2.707	2.047–2.197	2.332–2.724	2.082–2.263
(Å)	Mean: 2.507	Mean:2.138	Mean: 2.493	Mean: 2.117	Mean: 2.502	Mean: 2.165
M1-O	2.078–2.119	2.066–2.130	2.048–2.099	2.067–2.116	2.071–2.136	2.106–2.192
(Å)	Mean: 2.103	Mean: 2.088	Mean: 2.068	Mean: 2.087	Mean: 2.101	Mean: 2.146
Si-O (Å)	1.538–1.752	1.596–1.662	1.586–1.680	1.621–1.654	1.588–1.684	1.635–1.654
	Mean: 1.605	Mean: 1.634	Mean: 1.635	Mean: 1.638	Mean: 1.635	Mean: 1.647

between 2.081 Å (in $CaMgSi_2O_6$) and 2.101 Å (in $CaCoSi_2O_6$) [4]. In $CaCo_{1-x}Ni_xSi_2O_6$ solid solutions mean M1-O (M1 = Co, Ni) distances are between 2.082 Å (in $CaCoSi_2O_6$) and 2.031 Å (in $CaNiSi_2O_6$) [7]. All of these values are shorter than 2.12 Å, the limit value that explains the pink or red colour of compound containing octahedral Co(II) ions when the mean M − O distance is lower than 2.12 Å (such as pink $MgCo_{x-}Ni_{1-x}SiO_4$ ($0.25 \leq x \leq 1.0$) solid solutions with olivine structure) and the colour blue, violet, purple or green of material when is greater than this value (such as the blue-violet Co_2SiO_4) [8]. Differences in experimental conditions from refeences generate small differences in mean M1-O (M1 = Mg, Ni or Co) distances in bibliography.

Structural information of $CaMgSi_2O_6$, $CaNiSi_2O_6$ and $CaCoSi_2O_6$ with diopside structure are compared in Table 1. In $CaMSi_2O_6$ (M = Mg, Ni, Co) with diopside structure (monoclinic symmetry) Ca(II) occupies the M2 site and M the M1 site. In $MgMSiO_4$ (M = Mg, Ni, Co) with olivine structure (orthorhombic symmetry) preference of Mg(II) for the M2 site and Co(II) and Ni(II) for M1 site is detected [8]. M1 site is smaller in diopside structure than in olivine structure for each chromophore ion and a higher bond strength modifies the colour of materials. So, an increase of red amount in colouration can be expected in $CaCoSi_2O_6$ respect to $MgCoSiO_4$. These solid solutions fired at 1200 °C could be used in ceramic industry because $CaMgSi_2O_6$ diopside is stable at high temperatures (melting at 1391 °C) [5], $CaNiSi_2O_6$ melts incongruently to give liquid phase between 1338 °C and 1420 °C [9] and $CaCoSi_2O_6$ melts incongruently generating liquid phase in the 1165–1230 °C temperature range [9].

The presence of Mg(II) ions in $CaMSi_2O_6$ (M = Co(II), Mg(II), Ni(II)) solid solutions might enhance the work with a lower amount of Co(II) and Ni(II) ions than in $CaCoSi_2O_6$ and $CaNiSi_2O_6$. To the best of our knowledge, the development of colours in solid solutions including three divalent cations Mg(II), Ni(II) and Co(II) in M1 site of diopside structure have not been reported to date.

In phosphate structures the amount of cobalt can be minimised with the partial substitution of Co(II) or Ni(II) by Mg(II). Thus, the colour of purple pigment with the $Co_3P_2O_8$ structure can be obtained from the powdered $Mg_{2.5}Co_{0.5}P_2O_8$ composition fired at 1200 °C [10]. $Mg_xCo_{3-x}P_2O_8$ ($2.0 \leq x \leq 2.5$) solid solutions were considered the optimal compositions with the $Co_3P_2O_8$ structure for obtaining the characteristic cobalt blue in glazed tiles [10]. From glazed tiles prepared with 4% $Co_xNi_{3-x}P_2O_8$ ($0.0 = x \leq 3.0$) materials fired at 1000 °C, yellowish brown, brown, green and blue colourations are obtained. These materials may be used in ceramic industry to avoid the loss of oxygen obtained with the use of Co(II) oxides [11]. As part of our ongoing research motivated by these previous reports, within this context we investigated the possible formation of CaMg0.5CoxNi0.5-xSi2O6 solid solutions with diopside structure to reduce the toxic and expensive amounts of cobalt and nickel. The aims of the study are to obtain the structural characterization of these fired materials, to monitor the evolution of the colour of these materials with composition and temperature, and to test the colouring in samples enamelled with a commercial glaze given that the obtained materials might be used by the ceramic industry.

2. Experimental section

$CaMg_{0.5}Co_xNi_{0.5-x}Si_2O_6$ ($0.0 \leq x \leq 0.5$) compositions were synthesized from $CaCl_2{\cdot}2H_2O$ (Scharlau, extra pure), $MgCl_2{\cdot}6H_2O$ (Acros Organic, extra pure), $Ni(NO_3)_2{\cdot}6H_2O$ (Acros Organic, 99%), $Co(NO_3)_2{\cdot}6H_2O$ (Acros Organic, 99%) and SiO_2 colloidal (Scharlau, pure), via the chemical co-precipitation method.

Suspensions were prepared mixing the stoichiometric amount of SiO_2 with water. After the stoichiometric amounts of $CaCl_2{\cdot}2H_2O$, $MgCl_2{\cdot}6H_2O$, $Ni(NO_3)_2{\cdot}6H_2O$ and $Co(NO_3)_2{\cdot}6H_2O$, were added to these suspensions in continuous agitation. Green, brown or red suspensions obtained were vigorously stirred for 22 h at room temperature. The change of colour in suspensions depends of Ni(II):Co(II) ratio. Then, an ammonia aqueous solution (Panreac, 25%) was added with continuous stirring until reaching pH = 10. In these conditions, the solid amount increased, and the colour of the suspensions changed. Green suspension was obtained when x = 0 and dark bluish green suspensions when x > 0. The obtained materials were dried in air to evacuate only the water. The Si:Mg:Ni:Co molar ratio of the starting materials was preserved in this process. Green colloidal gels, solid material blocks formed by physical bonding of particles with solvent retention, were obtained. The colloidal gels were broken into smaller pieces to be placed in alumina crucibles and calcined at 300, 600, 800, 1000 and 1200 °C for 6 h at each temperature.

The development of the crystalline phases at different temperatures was studied by XRD. The resulting materials were examined using a Panalytical X-ray diffractometer (Malvern Panalytical, Almelo, The Netherlands) with CuK_α radiation. To follow the development of the diopside crystalline phase, the crystallinity was calculated as $C = [(I_a - I_b)/I_a]{\cdot}100$, where I_a is the background intensity around 29° 2θ and I_b is the intensity of the (−221) diffraction maximum for diopside crystalline structure. This expression is an approximation that does not consider the different factors that contribute to the phenomenon of X-ray diffraction, but it does give us an approximate idea of the evolution of the crystalline phase with composition and temperature. Additionally, the percentage of crystallinity from 5° to 80° of titled composition phases at different temperatures were calculated using the diffractometer software.

The unit cell parameters and interatomic distances in the developed structures were determined to investigate the possible formation of solid solutions under these synthesis conditions. A structure profile refinement was carried out via the Rietveld method (Fullprof.2k computer program) [12–14]. Diffraction patterns ranging between 6 and 110° (2θ) were collected employing monochromatic CuK_α radiation, a step size of 0.02° (2θ) and a sampling time of 10 s. Structural information of $CaMgSi_2O_6$ compound taken from the Inorganic Crystal Structure Database [15] was used as initial model in refinements. This database (ICSD) includes standard cell, standard space group, fractional atomic

Table 2
Crystalline phases in $CaMg_{0.5}Co_xNi_{0.5-x}Si_2O_6$ ($0.0 \leq x \leq 0.5$) compositions.

	800 °C	1000 °C	1200 °C
x = 0.0	D(m)	D(s), W(vw), M(w)	D(s), W(vw)
x = 0.1	D(m), W(vw)	D(s), W(vw), N(w)	D(s), W(vw), N(w)
x = 0.2	D(m), W(vw)	D(s), W(vw)	D(s), W(vw)
x = 0.3	D(m)	D(s), W(vw)	D(s), W(vw)
x = 0.4	D(m)	D(s), W(vw)	D(s), W(vw)
x = 0.5	D(m)	D(s), W(vw)	D(s), W(vw)

Crystalline phases: D = diopside, W = $CaSiO_3$ (parawollastonite), M = MO (M = Mg, Ni), N = $Mg_2Si_2O_6$.
Diffraction peak intensity: s = strong, m = medium, w = weak, vw = very weak.

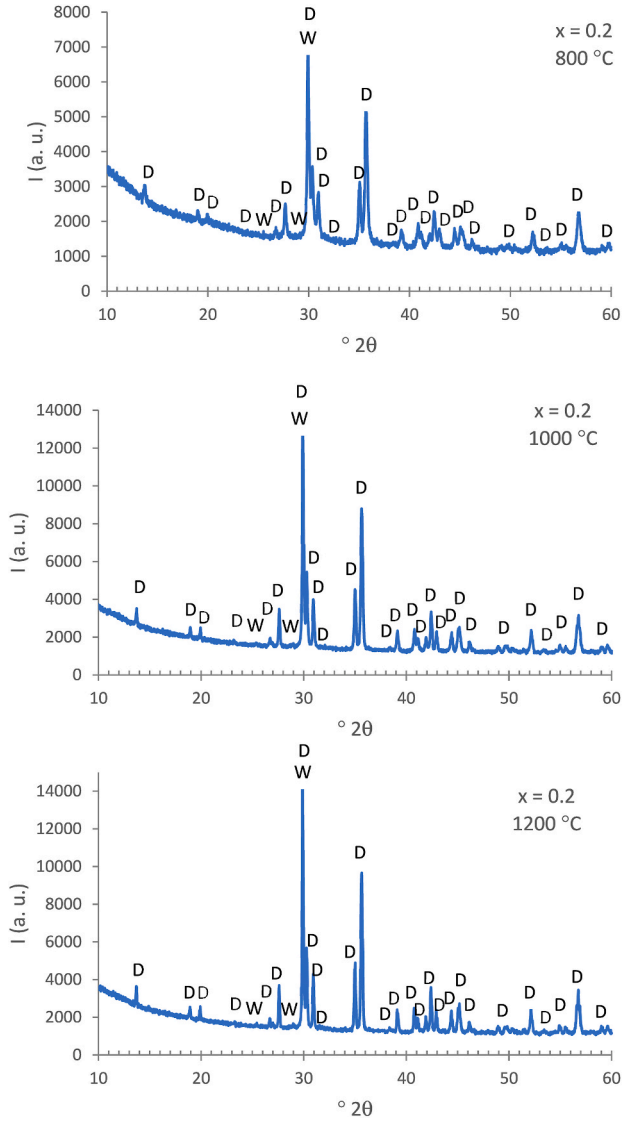

Fig. 1. Evolution of crystalline phases with temperature in $CaMg_{0.5}Co_{0.2}Ni_{0.3}Si_2O_6$ composition (D: diopside structure, W: $CaSiO_3$).

coordinates and other information on crystalline phases reported in the literature.

The Co(II) and Ni(II) sites and the transfer charge bands in the samples were studied by UV–vis–NIR spectroscopy (diffuse reflectance). The ultraviolet visible near infrared (UV–vis–NIR) spectra in the 200–2500 nm range were obtained using a Jasco V-670 spectrophotometer. To test the colour developed in glazes, the compositions fired at 1200 °C were 2% weight enamelled with a commercial glaze (SiO_2 - Al_2O_3 - PbO - Na_2O - CaO glaze) onto commercial ceramic biscuits. Many pigments are dissolved in this glaze. The colour of the material is lost or changes when this happens. Glazed tiles were fired for 15 min at 1065 °C, subsequently obtained their UV–vis–NIR spectra.

The CIE L*a*b* colour parameters on the fired samples: L* is the lightness axis (black (0) → white (100)), a* is the green (−) → red (+) axis, and b* is the blue (−) → yellow (+) axis [16] were obtained with a Jasco V-670 spectrophotometer (SP60, standard illuminate D65, an observer 10°, and a reference sample of MgO). The measurements were performed on powdered samples and on glazed tiles. Chroma ($C^* = \sqrt{[(a*)^2 + (b*)^2]}$) and tone ($H^* = tg^{-1}(b^*/a^*)$) were calculate from measure values of a* and b*. Chroma is the attribute that expresses the purity of a colour. Tone (synonym for hue, colour, shade, and tint) is the dominant wavelength of light that a person can see (yellow, red, blue, green, etc.). Mixing a pure hue with other colour reduces its purity and lowers its chroma.

XPS results indicating the oxidation states of the transition metals included in the studied composition were performed in a SPECS spectrometer using Al Kα (1486.6 eV).

Distribution of chemical elements in enamelled samples was studied by scanning electron microscopy (JEOL-6610LV) to test the dissolution or non-dissolution of the solid solutions prepared in the glaze. Microanalysis and EDX mapping from enamelled samples were obtained.

3. Results and discussion

Table 2 shows the evolution of the crystalline phases with temperature in $CaMg_{0.5}Co_xNi_{0.5-x}Si_2O_6$ ($0.0 \leq x \leq 0.5$) compositions. Diopside crystalline phase is detected at 800 °C, although a better crystallization (higher intensity) is obtained at 1000 and 1200 °C. The diopside (D) is the majority crystalline phase at these three temperatures. Traces of $CaSiO_3$ parawollastonite (ICSD-30884, S.G.: $P2_1/c$) are also detected in these temperatures. Small amounts of MO (M = Ni, Mg) with NaCl structure or $Mg_2Si_2O_6$ crystalline phases were also detected when x = 0.0 at 1000 °C or when x = 0.1 at 1000 and 1200 °C. At 1000 and 1200 °C the diffraction maxima are very intense and narrow. So, the 1000 and 1200 °C were considered adequate to work with these compositions.

Fig. 1 shows the evolution of crystalline phases with temperature in $CaMg_{0.5}Co_{0.2}Ni_{0.3}Si_2O_6$ (x = 0.2) composition. In it, the intensity of 6795 u.a. for the diffraction maximum about 29.9° 2θ observed at 800 °C increases with temperature (with intensities of 12943 and 14427 u.a. at 1000 and 1200 °C respectively). This diffraction maximum corresponds to (−221) crystal plane of diopside and to (023) crystal plane of wollastonite. The other diffraction lines of wollastonite are less intense than this diffraction maximum about 30 °2θ. Considering the non-overlapping diffraction lines can be stated that the contribution of the wollastonite at the diffraction line about 30 °2θ is very small.

The intensity ratio (I_1/I_2) of two diffraction lines about 29.5–30.0° 2θ (line with intensity I_1) and 35.5–35.6° 2θ (line with intensity I_2) are 1.31 at 800, 1.45 at 1000 and 1.48 at 1200 °C in $CaMg_{0.5}Co_{0.2}Ni_{0.3}Si_2O_6$ (x = 0.2) composition. This ratio changes with composition in

Table 3
Calculated values of crystallinity I (−221) and 5–80° (percentage) at different burning temperatures of $CaMg_{0.5}Co_xNi_{0.5-x}Si_2O_6$ ($0.0 \leq x \leq 0.5$) compositions.

X	Crystallinity, 29.5°–29.9° 2θ %			Crystallinity, 5°- 80° 2θ (%)		
	800 °C	1000 °C	1200 °C	800 °C	1000 °C	1200 °C
0.0	75.3	87.9	90.0	76.4	86.2	87.7
0.1	74.5	85.4	87.6	78.9	84.9	85.8
0.2	76.5	87.3	89.2	81.9	86.1	86.9
0.3	77.5	88.0	88.9	79.2	86.3	86.8
0.4	81.6	89.1	89.4	81.1	86.7	86.4
0.5	85.7	88.5	88.7	81.3	86.7	85.5

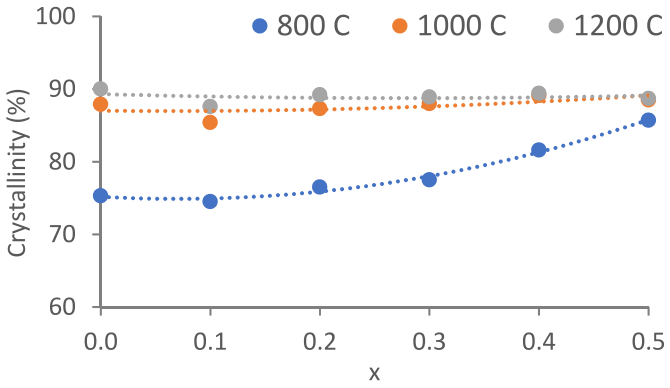

Fig. 2. Evolution of crystallinity with composition and temperature.

compounds with diopside structure. This ratio is 2.16 from $CaMgSi_2O_6$ (ICSD-52359), 1.26 from $CaNiSi_2O_6$ (ICSD202244), 1.07 from $CaCoSi_2O_6$ (ICSD-202245), 1.09 from $CaMg_{0.31}Co_{0.69}Si_2O_6$ (ICSD-263511) and 1.24 from $CaMg_{0.55}Ni_{0.45}Si_2O_6$ (ICSD-69383). So, the increasing from 1.31 to 1.48 seems to be in accordance with a higher incorporation of Mg(II) ions at 1000 and 1200 °C than at 800 °C because this intensity ratio is the highest in diopside $CaMgSi_2O_6$. A higher amount of Mg(II) ions might be also in amorphous phase at temperatures smaller than 1000 °C than at temperatures higher than 1000 °C.

Based on the (−221) crystal plane of diopside between 2θ of 29.5 and 29.9°, and the background intensity around 2θ of 29°, the crystallinity index was calculated for the $CaMg_{0.5}Co_xNi_{0.5-x}Si_2O_6$ ($0.0 \leq x \leq 0.5$) compositions (Table 3). The smallest crystallinity is obtained from $CaMg_{0.5}Ni_{0.5}Si_2O_6$ ($x = 0.0$) composition at 800 °C and it increases with temperature and x. When $x = 1.0$, the values of crystallinity are comparable at the three temperatures. The presence of Ni(II) in compositions decreases the crystallinity respect to $CaMg_{0.5}Co_{0.5}Si_2O_6$, mainly at 800 °C. The crystallinity obtained from the 5–80° 2θ range is smaller than the calculated from the maximum between 29.5 and 29.9° 2θ at 1000 and 1200 °C from all compositions and at 800 when $x \geq 0.4$. Differences between the crystallinity calculated in a narrow or wide range of 2θ is <6 % at 800 °C and <3,3 % at 1000 and 1200 °C. So, both forms provide a qualitative evolution of crystallinity with values from 75 % to 90 % in these compositions and temperatures. Furthermore, the percentage of crystallinity from 5 to 80° (2θ) of $CaMg_{0.5}Co_xNi_{0.5-x}Si_2O_6$ at different compositions and temperatures confirmed that the crystallinity increases with the increment of burning temperature as presented in (Table 3).

The evolution of crystallinity (obtained from the maximum between 29.5 and 29.9° 2θ) with composition and temperature is shown in Fig. 2. This figure shows than in these compositions crystallinity is lower at 800 °C than at 1000 and 1200 °C. At 800 °C increases with x (with Co(II) amount). A slight increase with x is detected at 1000 °C and no significant changes are observed at 1200 °C.

The crystalline structure of $CaMgSi_2O_6$ diopside with monoclinic structure, Z = 4, Space Group: *C*2/c (nº 15), contains Ca(II) and Mg(II) ions sited in 4e special positions (0, y, ¼) alternating along *b* direction with CN = 8 (M2 site) and CN = 6 (M1 site) respectively [15] (ICSD-52359). Si(IV) and three different crystallographic O(-II) ions are located in 8f general positions forming chains of tetrahedra SiO_4 which are linked to the CaO_8 and MgO_6 polyhedra. In the c-axis direction, CaO_8 polyhedra share edges with each other to form chains, MgO_6 polyhedra also share edges with each other to form chains in this direction, but SiO_4 tetrahedra only share vertices forming zig-zag chains in the c direction. In the direction of the b axis, some edges are also shared between the CaO_8 and MgO_6 polyhedra, leaving these polyhedra alternating in this direction. Fig. 3 shows the diopside structure. In Fig. 3a the unit cell has been extended in *b* direction to highlight the alternance of Ca(II) and M1(II) in this direction. The structure was drawn with the Studio program [12–14] from $CaMgSi_2O_6$, ICSD-52359 data. Ca-O bonds shorter than 2.8 Å, M1-O (M1 = Mg, Co, Ni) bonds shorter than 2.2 Å and Si-O bonds shorter than 1.8 Å are shown in Fig. 3

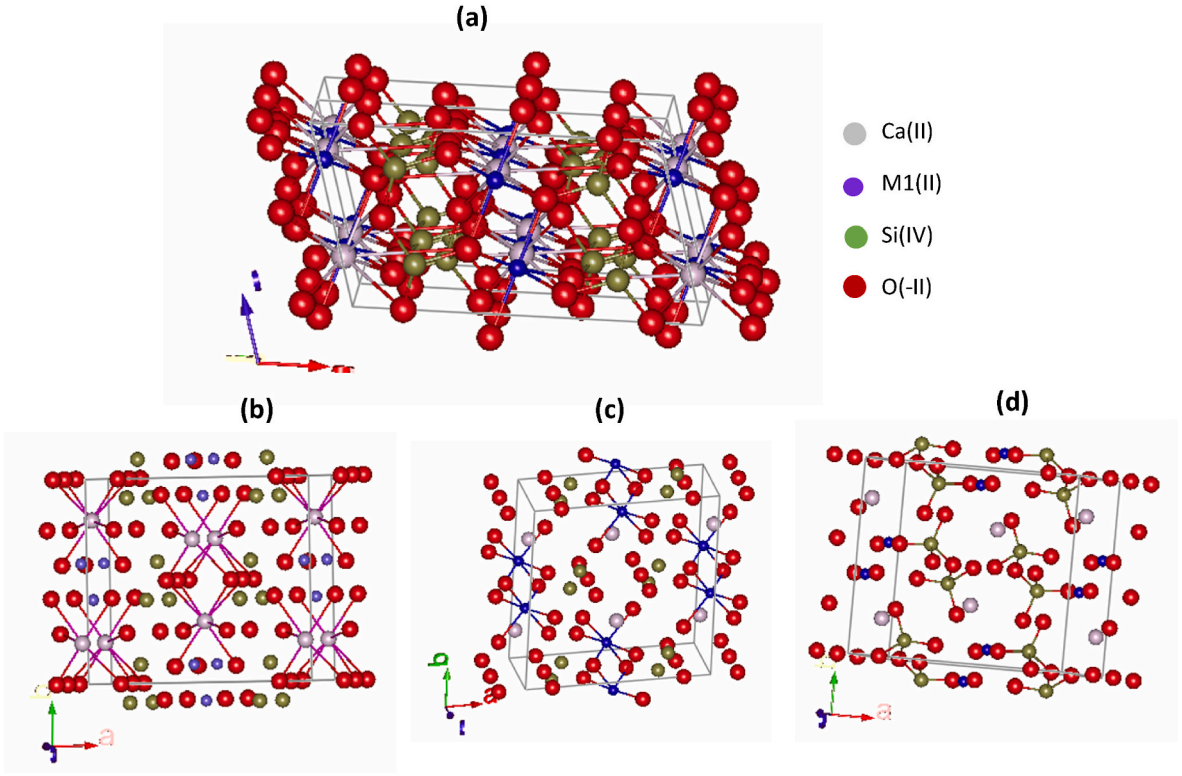

Fig. 3. Two unit cells of diopside structure showing alternance of Ca(II) and M1(II) in the b direction. (a) Ca-O bonds, (b) M1-O bonds (c) and Si-O bonds (d) in diopside structure. M1 = Mg, Co, Ni.

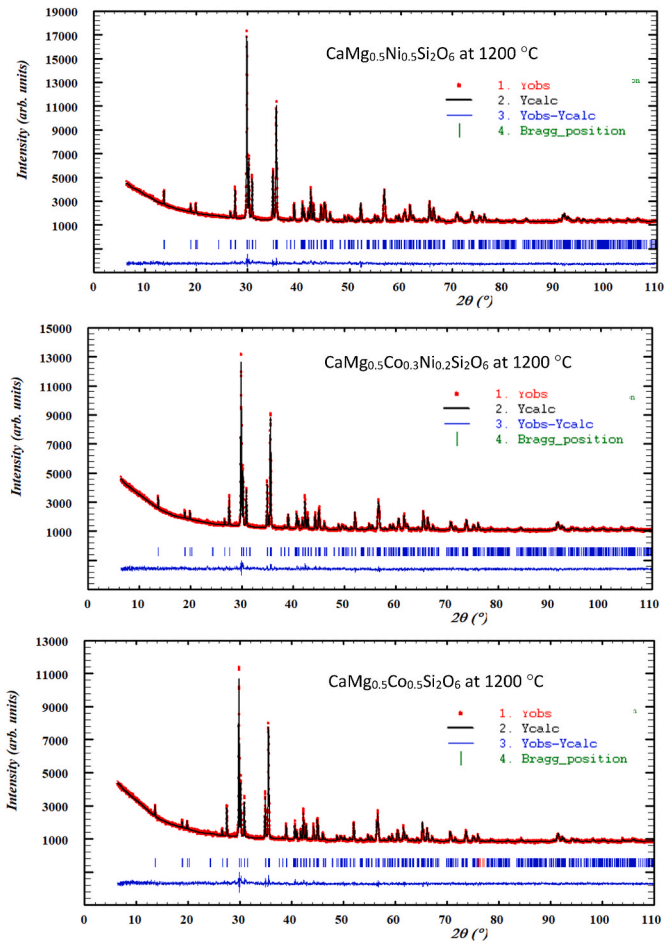

Fig. 4. The diffraction profile refinement of diopside structure from $CaMg_{0.5}Ni_{0.5-x}Co_xSi_2O_6$ (x = 0.0, 0.3, 0.5) compositions fired at 1200 °C by Rietveld's method.

Table 4
Unit cell parameters and volume in $CaMg_{0.5}Ni_{0.5-x}Co_xSi_2O_6$ compositions.

T (°)	x	a (Å)	b (Å)	c(Å)	β (°)	V (Å^3)
1000	0.0	9.7439 (2)	8.9176 (2)	5.2385(1)	105.851(1)	437.88(2)
1000	0.1	9.7528 (2)	8.9218 (2)	5.2374(1)	105.779(1)	438.54(2)
1000	0.2	9.7569 (1)	8.9283 (1)	5.2426(7)	105.779(8)	439.49(1)
1000	0.3	9.7652 (1)	8.9330 (9)	5.2452(6)	105.741(7)	440.391 (8)
1000	0.4	9.7693 (1)	8.9369 (1)	5.2471(6)	105.710(7)	440.998 (9)
1000	0.5	9.7749 (1)	8.9429 (1)	5.24851 (7)	105.6914 (8)	441.70(1)
1200	0.0	9.7429 (1)	8.9196 (1)	5.23806 (6)	105.833(6)	437.935 (9)
1200	0.1	9.7510 (2)	8.9220 (2)	5.2374(1)	105.790(1)	438.45(1)
1200	0.2	9.7563 (1)	8.9289 (1)	5.24215 (7)	105.7809 (8)	439.45(1)
1200	0.3	9.7626 (1)	8.9329 (1)	5.2438(6)	105.7412 (7)	440.150 (9)
1200	0.4	9.7691 (1)	8.9378 (1)	5.24602 (6)	105.7065 (7)	440.948 (8)
1200	0.5	9.7748 (1)	8.9437 (2)	5.24779 (6)	105.6771 (7)	441.707 (9)

(b), (c), and (d) respectively (Table 1).

In diopside structure, M2 is usually occupied by large Ca^{2+} cations and M1 is usually occupied by smaller cations such as Mn^{2+}, Fe^{2+}, Mg^{2+}, Fe^{3+}, Ni^{2+} or and Co^{2+}. Co^{2+} can be sited in M2 site only when compositions are Ca^{2+} deficient such as $(Ca_{0.2}Co_{0.8})CoSi_2O_6$ and in it can change from *C*2/c to the $P2_1/c$ symmetry [4,17].

A good structure profile fit from the $CaMg_{0.5}Co_xNi_{0.5-x}Si_2O_6$ ($0.0 \leq x \leq 0.5$) compositions fired at 1000 and 1200 °C was obtained with Ca(II) sited in M2 and Mg(II), Co(II) and Ni(II) sited in M1. The occupation of this M1 position was considered distributed proportionally to the stoichiometry of the composition. So, results are in accordance with the occupation of Ni(II) and Co(II) in M1 site together Mg(II) ions and no occupation of these ions in M2 site (Ca(II) site) is detected. The unit cell parameters and Ca-O, M1-O (M = Mg, Ni, Co) and Si-O interatomic distances were obtained with the diffraction profile refinement by the Rietveld method including these considerations. Fig. 4 shows graphical results of the diopside structure profile refinement carried out via the Rietveld method in x = 0, x = 0.3 and x = 0.5 compositions at 1200 °C. Bragg position marks to diopside structure are included in Fig. 4. Traces of $CaSiO_3$ were not considered in refinements at this temperature.

Table 4 shows unit cell parameters and volume in diopside structure obtained for $CaMg_{0.5}Co_xNi_{0.5-x}Si_2O_6$ ($0.0 \leq x \leq 0.5$) compositions at 1000 and 1200 °C. No significant variations between 1000 and 1200 °C were obtained. In both temperatures, *a* and *b* unit cell parameters in diopside structure increase with x in accordance with the replacement of Ni(II) by the bigger Co(II) (in octahedral coordination the Ni(II) radius is 0.830 Å and the high spin Co(II) radius 0.885 Å [18]). The *c* unit cell parameter also increases but the variation is very small. The β angle closes slightly as x increases ($\beta(CaNiSi_2O_6) = 105.87°$, $\beta(CaCoSi_2O_6) = 105.45°$, Table 1). The variation of unit cell parameters with composition (x) indicates the formation of solid solutions with diopside structure.

Fig. 5 compares the values of the unit cell parameters at 800, 1000 and 1200 °C. Differences in *a*, *b* and β parameters are detected in values at 800 °C and 1000 or 1200 °C. This fact and the lower intensity in diffractograms indicate that crystallization of diopside has not finished at 800 °C (Fig. 2). The variation of unit cell parameters with x is lineal according to Vegard's law indicating the random distribution of Mg(II), Ni(II) and Co(II) in M1 site when solid solutions are formed. The variation of b parameter is not parallel at different temperatures and the smallest value from x = 0.0 at 800 °C indicate the smallest average radius in M1 site. In octahedral coordination the Mg(II) radius is 0.860 Å, the Ni(II) radius 0.830 Å and the high spin Co(II) radius 0.885 Å [18]. From these values, the b parameter of $CaMg_{0.5}Ni_{0.5}Si_2O_6$ (x = 0.0) smaller at 800 °C than at 1200 °C can be explained by the incorporation of a higher amount of Ni(II) ions than Mg(II) ions in diopside structure at this temperature. So, the non-crystalline phase is enriched by Mg(II). This result was also detected from intensities ratio of the two more intense diffraction lines in diopside structure in fired $CaMg_{0.5}Co_{0.2}Ni_{0.3}Si_2O_6$ (0.2) composition discussed above.

Fig. 6 shows the interatomic distances of $CaMg_{0.5}Co_xNi_{0.5-x}Si_2O_6$ ($0.0 \leq x \leq 0.5$) solid solutions with diopside structure at 1200 °C. Small variations with composition are observed in each distance. This figure shows the difference between the four large Ca-O3 distances with respect to the other four Ca-O1 and Ca-O2 distances in M2 site. Distortion of octahedral M1 site, with two M1-O1 and two M1-O2 distances shorter than the other two M1-O1 distances, is maintained with the variation of the composition. All M1-O distances obtained fall within the range 2.05–2.14 Å. In this structure, distortion in the tetrahedral site is greater than in the octahedral site.

Fig. 7 shows UV–vis–NIR spectra of Co_3O_4 with spinel structure (commercial raw material) and $CaMg_{0.5}Co_xNi_{0.5-x}Si_2O_6$ ($0.0 \leq x \leq 0.5$) compositions at 600 and 800 °C. At 600 °C, bands are poorly defined and spectra is similar to Co_3O_4 spectra in compositions with a higher initial Co(II) amount. So, in these compositions, the absorbance in all the wavelengths (grey colour) is associated with the presence of Co_3O_4.

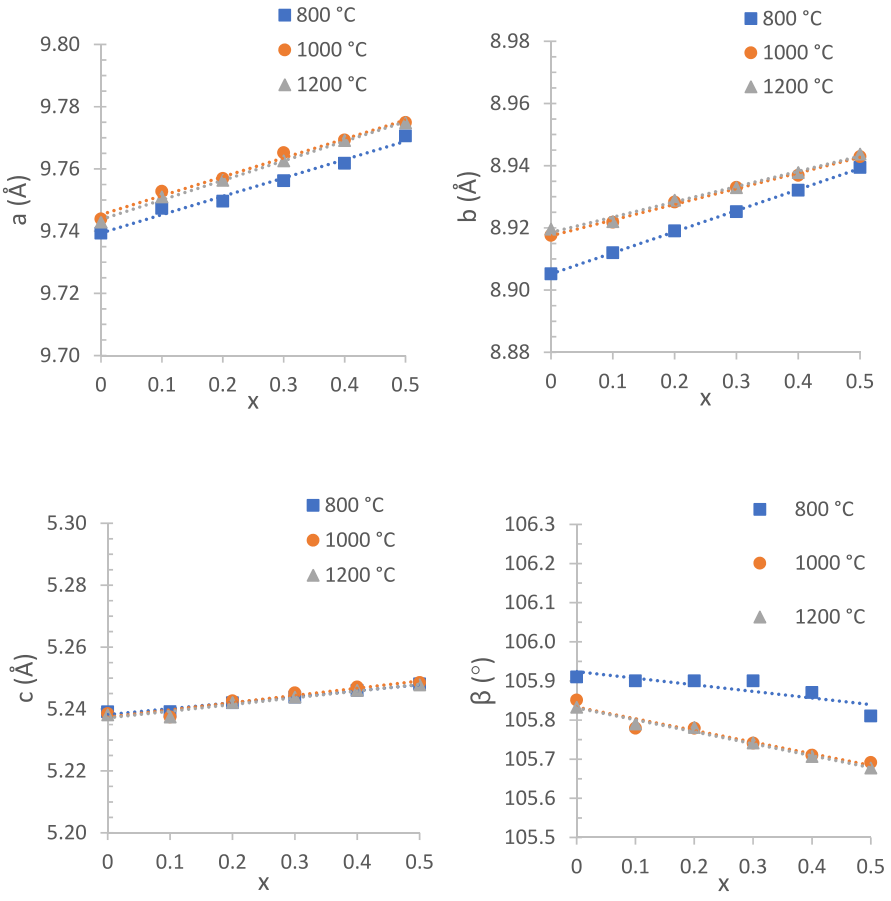

Fig. 5. Unit cell parameters of diopside structure in $CaMg_{0.5}Ni_{0.5-x}Co_xSi_2O_6$ compositions fired at 800, 1000 and 1200 °C.

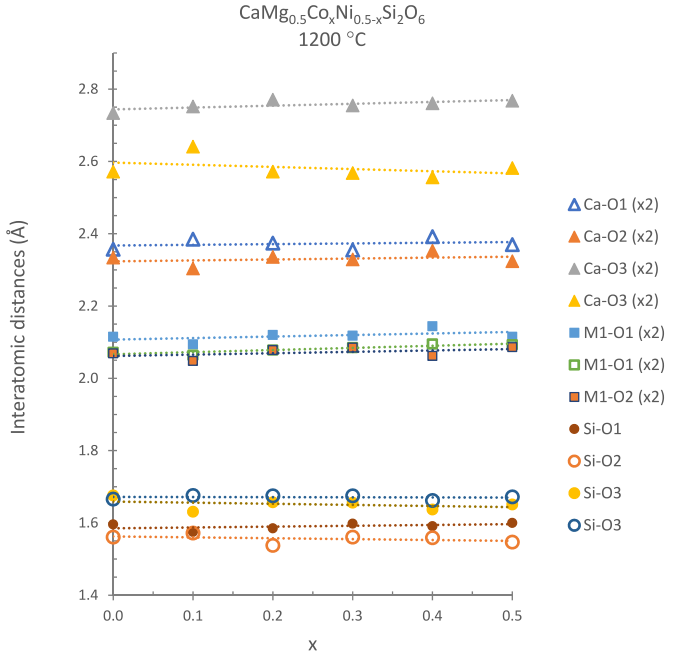

Fig. 6. Interatomic distances of $CaMg_{0.5}Co_xNi_{0.5-x}Si_2O_6$ solid solutions with diopside structure at 1200 °C. M1 = Mg(II), Ni(II) and Co(II).

Co_3O_4 with spinel structure contains tetrahedral Co(II) ions and octahedral Co(III) (ICSD-624573). $^4A_2 \rightarrow {}^4T_1(P)$ transition of tetrahedral Co (II) ions, $^1A_1 \rightarrow {}^1T_1$ and $^1A_1 \rightarrow {}^1T_2$ transitions of octahedral Co(III) ions can be assigned to absorbances about 450 and 700 nm. In these wavelengths also is described the presence of O^{2-} - Co^{2+} (~410 nm) and O^{2-} - Co^{3+} (~720 nm) charge transfer bands [19]. The strong absorbance between 1250 and 1500 nm can be assigned to octahedral Co(II) and it is in accordance with the disordered spinel at high temperature (T > 912 °C): $(Co^{2+}_{1-x}\ Co^{3+}_x)[Co^{2+}_x\ Co^{3+}_{2-x}]O_4$ [20]. At 800 °C, bands are defined in spectra and bands can be assigned to octahedral Ni(II) and Co(II) ions in the diopside structure. Bands at 1226, 774 and 422 nm are assigned to $^3A_2 \rightarrow {}^3T_2(F)$, $^3A_2 \rightarrow {}^3T_1(F)$ and $^3A_2 \rightarrow {}^3T_1(P)$ transitions in octahedral Ni (II). Bands at 1338, 705 and 538 nm are assigned to $^4T_1 \rightarrow {}^4T_2$, $^4T_1 \rightarrow {}^4A_2$ and $^4T_1 \rightarrow {}^4T_1(P)$ transitions in octahedral Co(II). Crystallization of diopside structure is detected at this temperature and the colour of samples changes from grey at 600 °C (due to the presence of Co_3O_4) to violet-pink ($0.1 \leq x \leq 0.4$) or pink ($x = 0.5$) at 800 °C (due to the presence of diopside structure) when $x \neq 0.0$. The colour of samples containing Co(II) ions is also pink at 1000 and 1200 °C. Bands assigned to octahedral Ni(II) and Co(II) ions in the diopside structure are also detected when temperature increases. Position of these bands at 1000 and 1200 °C is similar to those obtained at 800 °C (Fig. 8). The maximum absorbance is detected at 1200 °C. The difference between the smallest and longest Co-O distances is minor in diopside structure than in olivine structure (0.065 Å in $CaCoSi_2O_6$ and 0.086 Å in $MgCoSiO_4$, Table 1). This minor distortion of the CoO_6 octahedra in diopside structure is observed as a minor width of band assigned to the third transition of octahedral Co(II), $^4T_1 \rightarrow {}^4T_1(P)$, that in $CaMg_{0.5}Co_xNi_{0.5-x}Si_2O_6$ solid solutions with diopside structure appears between 460 and 580 nm, while in $MgCo_xNi_{1-x}SiO_4$ solid solutions with olivine

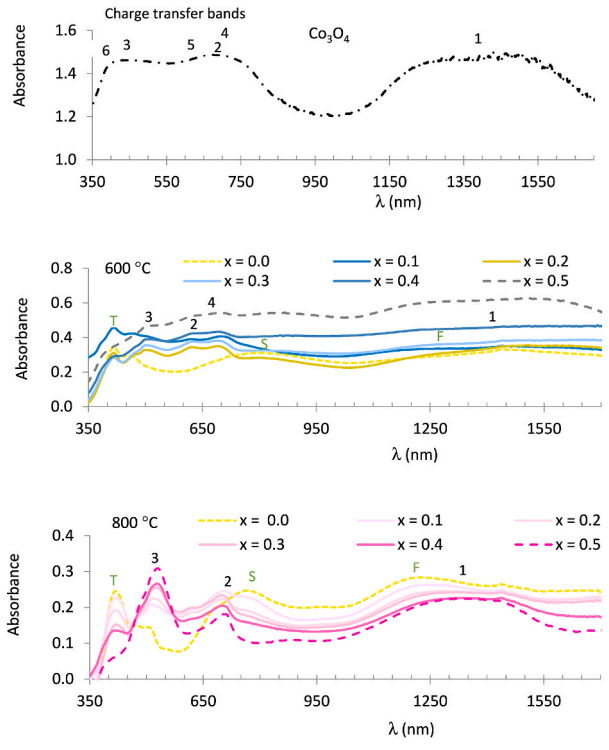

Fig. 7. UV–vis–NIR spectra of spinel Co_3O_4 and $CaMg_{0.5}Co_xNi_{0.5-x}Si_2O_6$ ($0.0 \leq x \leq 0.5$) compositions at 600 °C and 800 °C. Ni(II) CN = 6: (F) $^3A_2 \rightarrow {}^3T_2(F)$, (S) $^3A_2 \rightarrow {}^3T_1(F)$, (T) $^3A_2 \rightarrow {}^3T_1(P)$. Co(II) CN = 6: (1) $^4T_1 \rightarrow {}^4T_2$, (2) $^4T_1 \rightarrow {}^4A_2$, (3) $^4T_1 \rightarrow {}^4T_1(P)$. Co(II) CN = 4 (tetrahedral coordination): (4) $^4A_2 \rightarrow {}^4T_1(P)$. Co(III) CN = 6: (5) $^1A_1 \rightarrow {}^1T_1$, (6) $^1A_1 \rightarrow {}^1T_2$.

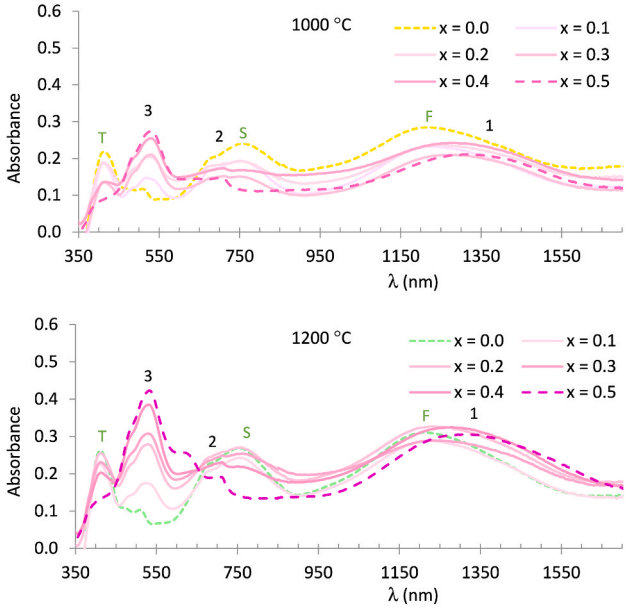

Fig. 8. UV–vis–NIR spectra of $CaMg_{0.5}Co_xNi_{0.5-x}Si_2O_6$ ($0.0 \leq x \leq 0.5$) solid solutions at 1000 °C and 1200 °C. Ni(II) CN = 6: (F) $^3A_2 \rightarrow {}^3T_2(F)$, (S) $^3A_2 \rightarrow {}^3T_1(F)$, (T) $^3A_2 \rightarrow {}^3T_1(P)$. Co(II) CN = 6: (1) $^4T_1 \rightarrow {}^4T_2$, (2) $^4T_1 \rightarrow {}^4A_2$, (3) $^4T_1 \rightarrow {}^4T_1(P)$.

structure this band appears between 450 and 600 nm [8]. So, the position of this band is centred into the green absorption range and the observed colour is pink (Fig. 8) and in $MgCo_xNi_{1-x}SiO_4$ solid solutions with olivine structure due to the extension of this band to yellow

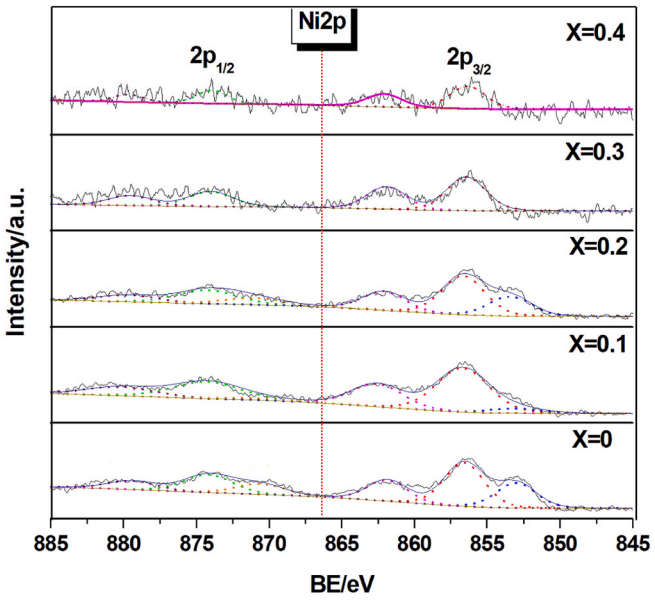

Fig. 9. Peak fitting result of Ni $2p_{1/2}$ and Ni $2p_{3/2}$.

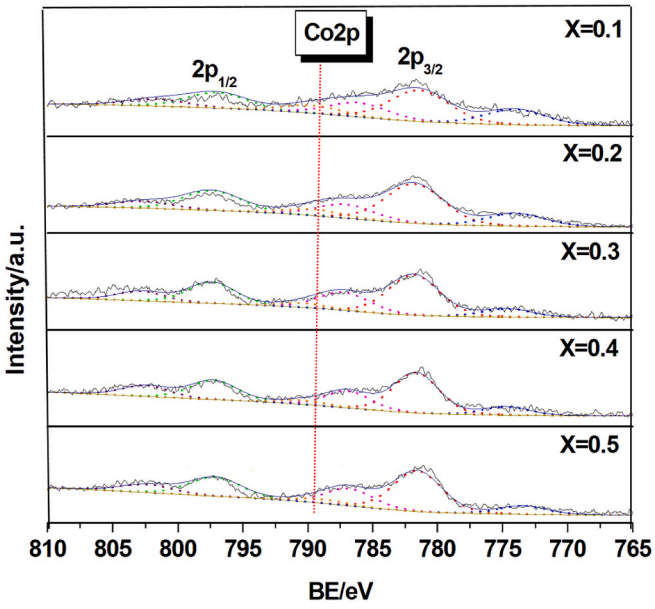

Fig. 10. Peak fitting result of Co $2p_{1/2}$ and Co $2p_{3/2}$.

absorption range, the observed colour is pink with a violet hue [8].

Figs. 9 and 10 show the XPS spectra obtained from samples fired at 1200 °C in 845–885 eV (Ni 2p) and 765–810 eV (Co 2p) respectively. At slightly higher energy than the energy of peaks $2p_{1/2}$ and $2p_{3/2}$ a satellite is assigned according to literature [21]. Two peaks corresponding to $2p_{1/2}$ and $2p_{3/2}$ can be observed in these spectra. The Ni $2p_{1/2}$ peak and the Ni $2p_{3/2}$ peak (Fig. 9) can be deconvoluted in two peaks in $0 \leq x \leq 0.2$ compositions containing a higher Ni amount. The Ni2p satellite peak is unaffected by the nature of ligand whereas the main peak is strongly affected but the Ni2p main line binding energy reflects the energetic properties of the ligand [22]. So, the presence of the maximum of these subpeaks at 873 and 870 eV from Ni $2p_{1/2}$ and at 856 and 852.5 eV from Ni $2p_{3/2}$ in these compositions can be related with two different contributions of the oxide ions in the diopside structure. The binding energy splitting is reported from NiO (855.6 and 854 eV) [21]. The

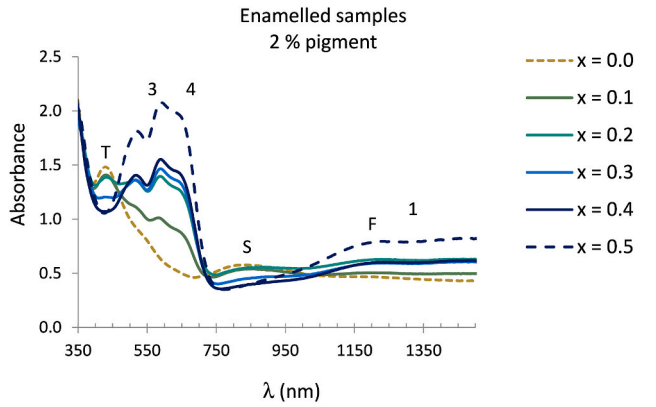

Fig. 11. UV–vis–NIR spectra of enamelled samples with 2% of $CaMg_{0.5}Co_xNi_{0.5-x}Si_2O_6$ ($0.0 \leq x \leq 0.5$) solid solutions fired at 1200 °C. Ni(II) CN = 6: (F) $^3A_2 \rightarrow {}^3T_2$, (S) $^3A_2 \rightarrow {}^3T_1$, (T) $^3A_2 \rightarrow {}^3T_1$(P). Co(II) CN = 6: (1) $^4T_1 \rightarrow {}^4T_2$, (2) $^4T_1 \rightarrow {}^4A_2$, (3) $^4T_1 \rightarrow {}^4T_1$(P). Co(II) CN = 4 (tetrahedral coordination): (4) $^4A_2 \rightarrow {}^4T_1$(P).

deconvolution of the Co $2p_{1/2}$ peak and the Co $2p_{3/2}$ peak can be observed from Fig. 10. The subpeaks at 797.5 and 790 eV from Co $2p_{1/2}$ and at 781 and 773 eV from Co $2p_{3/2}$ could indicate the presence of a small amount of Co(III) in compositions [21].

Fig. 11 shows the UV–vis–NIR spectra in glazed tiles prepared with 2% $CaMg_{0.5}Co_xNi_{0.5-x}Si_2O_6$ ($0.0 \leq x \leq 0.5$) solid solutions fired at 1200 °C. The increase of absorbance at 455–695 nm with the presence of a new band at 657 nm is observed in the enamelled samples spectra when $x > 0.0$ (in all samples containing cobalt). This band can be assigned to tetrahedral Co(II) ion, $^4A_2 \rightarrow {}^4T_1$ (P), and is responsible for the blue component in the colour of the enamelled samples. Band at 425 nm assigned to third transition of octahedral Ni(II), $^3A_2 \rightarrow {}^3T_1$(P), is responsible for the yellow component in the colour of the enamelled samples. So, enamelled samples when $0.1 \leq x \leq 0.2$ are green and when $0.3 \leq x \leq 0.5$ are blue. The lower absorbance in $\lambda > 725$ nm than in $\lambda < 725$ nm is in accordance with the dissolution of the solid solutions in glazes. The first transition of octahedral Ni(II) in the enamelled $CaMg_{0.5}Ni_{0.5}Si_2O_6$ composition and the second transition of octahedral Co(II) in the enamelled $CaMg_{0.5}Co_{0.5}Si_2O_6$ composition are indistinguishable from spectra. So, these $CaMg_{0.5}Co_xNi_{0.5-x}Si_2O_6$ solid solutions might be used as pink pigments in paints and to obtain green or blue materials in ceramic industry. These solid solutions contain lower amounts of the toxic and expensive of nickel and cobalt than Ni_2SiO_4 and Co_2SiO_4 and develop deep colours in glazes.

The evolution of the colour of $CaMg_{0.5}Co_xNi_{0.5-x}Si_2O_6$ ($0.0 \leq x \leq 0.5$) solid solutions is shown in Fig. 12. The green ($x < 0.3$) or brown ($x \geq 0.3$) colour of colloidal gels turns yellow ($x = 0.0$) or blue ($0.2 \leq x \leq 0.5$) at 300 °C. At 600 °C, beige ($x = 0.0$), brown ($x = 0.1$) and grey colour were obtained in compositions. The grey colour can be associated with the presence of Co_3O_4 in these compositions with a strong charge transfer band in visible spectra (Fig. 7). The colour of samples with $x > 0.0$ turns violet-pink ($0.1 \leq x \leq 0.4$) or pink ($x = 0.5$) at 800 °C. This change of colour coincides with a better band definition in spectra

Fig. 12. The colour images of prepared dried gels and fired $CaMg_{0.5}Co_xNi_{0.5-x}Si_2O_6$ ($0.0 \leq x \leq 0.5$) compositions. (For interpretation of the references to colour in this figure legend, the reader is referred to the Web version of this article.)

Table 5
CIE L*a*b* parameters, chroma (C*), hue (H*) and observed colour from $CaMg_{0.5}Co_xNi_{0.5-x}Si_2O_6$ compositions.

x		Colloidal gels	300 °C	600 °C	800 °C	1000 °C	1200 °C
0.0	L*	50.07	45.58	82.50	89.91	94.49	92.31
	a*	−22.21	−29.73	+0.69	−1.71	−3.44	−5.18
	b*	+9.75	+20.61	+13.10	+8.32	+5.54	+7.71
	C*	24.26	36.18	13.12	8.49	6.52	9.29
	H*	156.30	145.27	86.89	101.62	121.84	123.90
	Colour	Green	Yellow	Beige	Yellow	Yellow	Pale green
0.1	L*	43.21	27.34	70.88	81.23	90.57	89.08
	a*	−7.71	−6.67	+1.24	+0.12	+2.55	+2.68
	b*	+15.99	+2.60	+7.09	−0.75	+0.77	+0.65
	C*	17.75	7.16	7.20	0.76	2.66	2.76
	H*	115.74	158.71	5.72	279.09	16.80	13.63
	Colour	Dark green	Green	Brown	Violet-Pink	Pink	Pink
0.2	L*	36.15	26.94	75.83	83.11	87.52	83.63
	a*	−1.92	−0.24	−0.38	+4.22	+5.17	+8.80
	b*	+14.10	−1.47	+0.38	−5.28	−2.35	−1.55
	C*	14.23	1.49	0.54	6.76	5.68	8.94
	H*	97.76	260.73	135	308.63	359.54	350.01
	Colour	Dark green	Blue	Grey	Violet-Pink	Pink	Pink
0.3	L*	26.47	26.00	73.88	84.42	86.14	83.02
	a*	+2.14	+1.44	−0.49	+6.27	+8.12	+13.27
	b*	+10.95	−5.45	−2.74	−7.90	−5.04	−5.46
	C*	11.16	5.64	2.78	10.09	9.56	14.35
	H*	78.94	284.8	259.86	308.44	328.17	337.63
	Colour	Brown	Blue	Grey	Violet-Pink	Pink	Pink
0.4	L*	32.93	22.80	70.73	83.91	83.82	77.49
	a*	+6.09	+1.42	−0.85	+10.17	+10.44	+16.89
	b*	+11.71	−5.02	−4.54	−8.70	−6.51	−9.28
	C*	13.20	5.22	4.62	13.38	12.30	19.27
	H*	62.52	285.8	259.39	319.45	328.05	331.22
	Colour	Brown	Blue	Grey	Violet-Pink	Pink	Pink
0.5	L*	30.96	34.69	63.78	83.74	83.57	74.59
	a*	+8.24	+2.08	−1.79	+18.81	+13.91	+18.35
	b*	+9.38	−9.46	−5.84	−13.79	−9.53	−15.91
	C*	12.49	9.69	6.11	23.32	16.86	24.29
	H*	48.70	282.4	252.96	323.76	325.59	319.08
	Colour	Brown	Blue	Dark grey	Pink	Pink	Pink

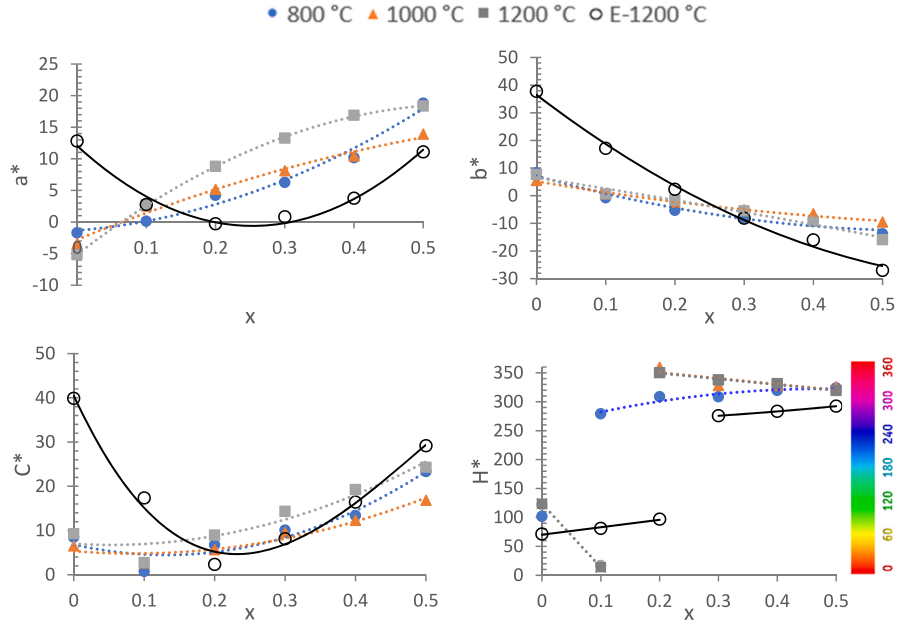

Fig. 13. CIE a* and b* colour parameters from $CaMg_{0.5}Co_xNi_{0.5-x}Si_2O_6$ solid solutions with diopside structure. (For interpretation of the references to colour in this figure legend, the reader is referred to the Web version of this article.)

(Fig. 7) and the presence of diopside as main crystalline phase in XRD (Table 2 and Fig. 1). At 1000 and 1200 °C all compositions with x > 0.0 are pink materials. This pink solid solutions show well defined bands in spectra (Fig. 8) and strong intensity of diopside crystalline phase in XRD (Table 2 and Fig. 4).

Table 5 shows the evolution of CIE L*a*b* parameters, chroma (C*),

Table 6
CIE L*a*b* colour parameters, chroma (C*), hue (H*) and observed colour from glazed tiles obtained from $CaMg_{0.5}Co_xNi_{0.5-x}Si_2O_6$ ($0.0 \leq x \leq 0.5$) solid solutions fired at 1200 °C.

x	L*	a*	b*	C*	H*	Observed colour
0.0	48.46	+12.82	+37.76	39.88	71.25	Beige
0.1	36.44	+2.76	+17.15	17.37	80.86	Brownish green
0.2	25.98	−0.28	+2.32	2.34	96.88	Dark green
0.3	22.06	+0.82	−8.11	8.15	275.77	Dark blue
0.4	22.23	+3.77	−15.97	16.41	283.28	Dark blue
0.5	16.06	+11.09	−26.99	29.18	292.34	Dark blue

hue (H*) and observed colour with composition and temperature of powdered $CaMg_{0.5}Co_xNi_{0.5-x}Si_2O_6$ compositions. The variation of C* shows a minimal value in composition with $x = 0.2$ at $T < 800$ °C (diopside structure is not detected at these temperatures) and in composition with $x = 0.1$ at $T \geq 800$ °C (diopside structure is developed at these temperatures). At $T \geq 800$ °C, yellow and green colours are observed when $x = 0.0$ (H* between 60 and 120°, between yellow and green) and pink colour when $x \neq 0$ (H* between 0 and 60°, between red and yellow colours or H* between 300 and 360°, between pink and red colours). When $x \neq 0$, the a* colour parameter (red amount (+)) increases with both composition (x) and temperature while b* colour parameter (yellow (+) to blue(−)) decreases with x. So, red and blue amount increases when Co(II) amount increases in these diopside solid solutions (Fig. 13). Pink is the observed colour due to the absorbance of the third transition of octahedral Co(II) responsible of the red colour ($^4T_1 \rightarrow {}^4T_1(P)$ at 538 nm) is highest. This pink colour is due to a mixture of red and white colours. Prepared compositions in this study include a maxima amount of 0.5 mol of Co(II) in octahedral site of diopside structure (red colour) and 0.5 mol of Mg(II) in the same position (white colour). Comparing pink colours of $MgCo_xNi_{1-x}SiO_4$ and $CaMg_{0.5}Co_xNi_{0.5-x}Si_2O_6$ solid solutions with olivine [8] and diopside (in this study) structures, the pink obtained with the diopside structure has a greater red amount than the pink obtained with the olivine structure with a smaller Co(II) amount in diopside structure. This fact can be explained by the mean M − O distance and octahedral distortion smaller in diopside structure than in olivine structure.

Table 6 includes CIE L*a*b* parameters, chroma (C*), hue (H*) and observed colour in $CaMg_{0.5}Co_xNi_{0.5-x}Si_2O_6$ enamelled samples. The variation of C* shows a minimal value in composition with $x = 0.2$ and H* values are between 60° (yellow) and 120° (green) when $x \leq 0.20$ and between 240° (violet) and 300° (pink) when $x \geq 0.3$ (Fig. 13). Green and blue colourations obtained when solid solutions were dissolved in the commercial glaze tested are similar to those obtained in the $MgNiSiO_4$ - $MgCoSiO_4$ and $Ni_2P_2O_7$ - $Co_2P_2O_7$ systems [8,23]. In $Mg_3P_2O_8$ - $Co_3P_2O_8$ system similar blue component is obtained although the red component is smaller than those obtained in this study [10].

Fig. 14 shows the distribution of Si, Ni and Co obtained by SEM/EDX mapping analysis on enamelled samples with 2% of $CaMg_{0.5}Co_xNi_{0.5-x}Si_2O_6$ ($0.0 \leq x \leq 0.5$) solid solutions fired at 1200 °C. Particles rich in Si can be observed but both Ni and Co are homogeneously distributed in samples according with their diffusion in glaze. The colour of the enamelled samples is attributed to Co(II) and Ni(II) ions in the glaze.

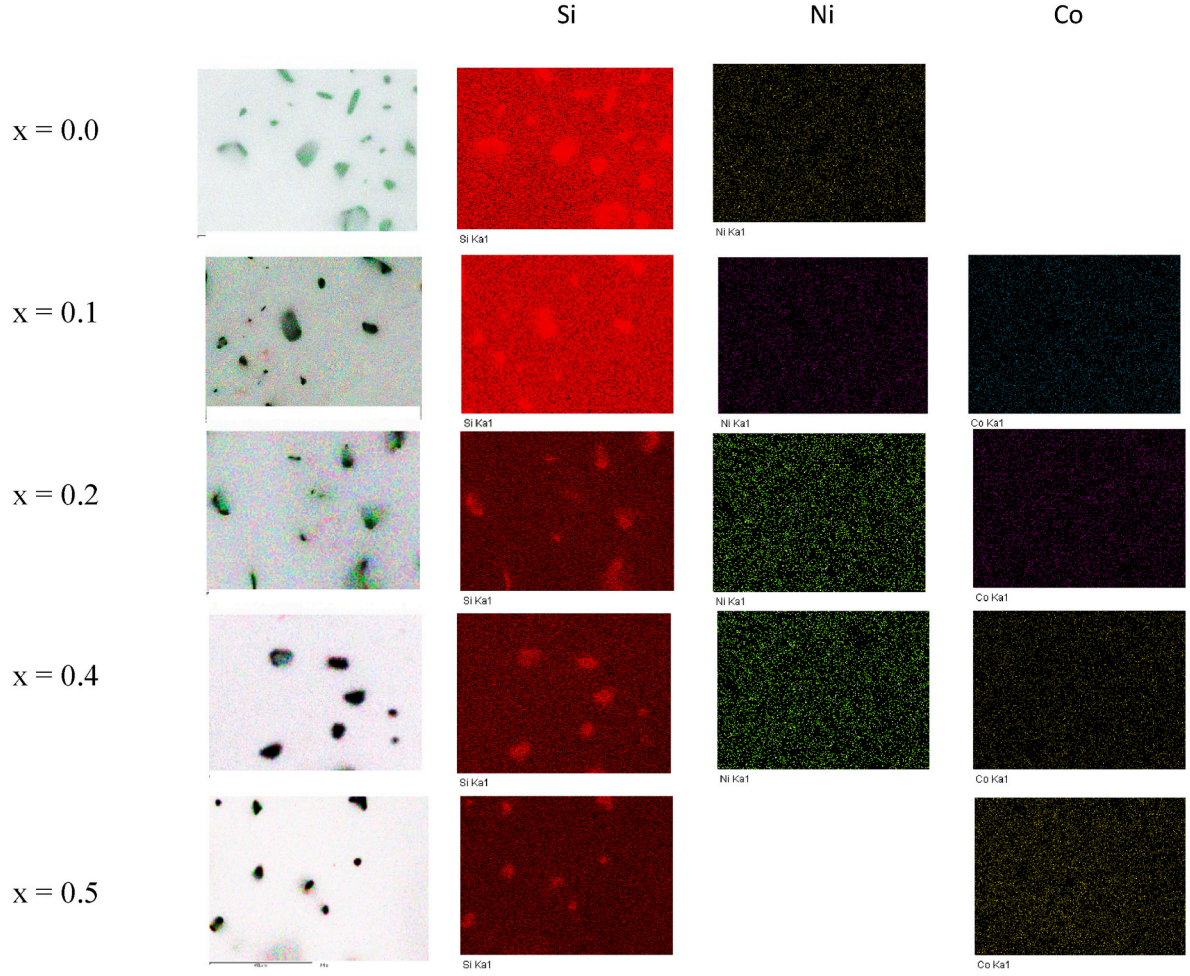

Fig. 14. Distribution of Si, Ni and Co in enamelled samples, with 2% of $CaMg_{0.5}Co_xNi_{0.5-x}Si_2O_6$ ($0.0 \leq x \leq 0.5$) solid solutions fired at 1200 °C, obtained by SEM/EDX mapping analysis.

Colour in $CaMg_{0.5}Co_xNi_{0.5-x}Si_2O_6$ enamelled samples is comparable to the enamelled samples with 2% $MgCo_xNi_{1-x}SiO_4$ solid solutions with olivine structure [13] but clarity in enamelled samples with 2% $CaMg_{0.5}Co_xNi_{0.5-x}Si_2O_6$ solid solutions with diopside structure is higher in these last one. The smaller Co(II) and Ni(II) amount can explain this higher clarity and $CaMg_{0.5}Co_xNi_{0.5-x}Si_2O_6$ pigments with diopside structure might be used in ceramic industry. For example, %-weight of Co(II) in $CaMg_{0.5}Co_{0.5}Si_2O_6$ composition is 12.6 while in $MgCoSiO_4$ composition is 33.7, although the decrease of Co(II) amount is possible in both structures with an increase of Mg(II) amount. These compositions might to avoid problems to work with great amounts of Co(II) or Ni (II) in the ceramic industry process obtaining intense green and blue colours. The use of a smaller amount of Co(II) and Ni(II) also to make less expensive the production of the pigments that developed similar colourations in enamelled samples. Authors think that the optimization of composition of the pigments is better than the decrease of the % of pigment added to frits, glazes or inks.

4. Conclusions

$CaMg_{0.5}Co_xNi_{0.5-x}Si_2O_6$ ($0.0 \leq x \leq 0.5$) solid solutions with diopside structure were synthesized at 1000 and 1200 °C. The variation of unit cell parameters with x is lineal according to Vegard's law indicating the random distribution of Mg(II), Ni(II) and Co(II) in M1 site when solid solutions are formed. At 1200 °C, a slight increase of the interatomic distances in diopside structure with composition is observed (mean M1-O distances between 2.085 Å for $x = 0.0$ and 2.098 Å for $x = 0.5$). Distortion of octahedral M1 site in diopside structure is lower than in olivine structure and it is maintained with the variation of the composition.

Crystallization of diopside structure is accompanied by change of the colour in samples from grey at 600 °C (due to the presence of Co_3O_4) to violet-pink ($0.1 \leq x \leq 0.4$) or pink ($x = 0.5$) at 800 °C (due to the presence of diopside structure) when $x \neq 0.0$. The colour of samples containing Co(II) ions is also pink at 1000 and 1200 °C because the position of the third transition band of octahedral Co(II), $^4T_1 \rightarrow {}^4T_1(P)$, is centred into the green absorption range (red colour observed with H* between 350.01° and 319.08° and a* between + 8.80 and +18.35 for $x = 0.2$ and $x = 0.5$ respectively).

Green and blue colourations were obtained from $CaMg_{0.5}Co_xNi_{0.5-x}Si_2O_6$ enamelled samples. These colourations are similar to those obtained in the $MgNiSiO_4$ - $MgCoSiO_4$ and $Ni_2P_2O_7$ - $Co_2P_2O_7$ systems when solid solutions were dissolved in the commercial glaze tested. The $CaMg_{0.5}Co_xNi_{0.5-x}Si_2O_6$ pigments with diopside structure might be used in ceramic industry with a 12.6 %-weight of Co(II) in $CaMg_{0.5}Co_{0.5}Si_2O_6$ composition while in $MgCoSiO_4$ composition is 33.7 %-weight of Co(II).

Declaration of competing interest

The authors declare that they have no conflict of interest.

Acknowledgements

We gratefully acknowledge the financial support provided by Spain's Agencia Estatal de Investigación. Ministerio de Ciencia e Innovación, PID2020-113558RB-C41, Principality of Asturias IDI/2021/50997 and CrysFact Network Red2018-10102574-T (AEI/MCI).

References

[1] V.M. Pogrebenkov, M.B. Sedel'nikova, V.I. Vereshchagin, Production of ceramic pigments with diopside structure from talc, Glass Ceram. 55 (5 – 6) (1998) 148–150.
[2] M.B. Sedel'nikova, V.M. Pogrebenkov, N.V. Liseenko, V.V. Gorbatenko, Nonstoichiometric reactions producing ceramic, Glass Ceram. 68 (3 – 4) (2011) 76–79.
[3] M.B. Sedel'nikova, V.M. Pogrebenkov, Production of Ceramic pigments with diopside and anorthite structure using the gel method, Glass Ceram. 63 (7 – 8) (2006) 271–273.
[4] C. Gori, M. Tribaudino, F. Mezzadri, H. Skogby, U. Hålenius, Co^{2+}-doped diopside: crystal structure and optical properties, Phys. Chem. Miner. 45 (2018) 443–461, https://doi.org/10.1007/s00269-017-0932-z.
[5] C. Gori, M. Tribaudino, L. Mantovani, G.D. Gatta, D. Delmonte, E. Gilioli, F. Mezzadri, G. Calestani, Synthesis and crystal structure of C2/c $Ca(Co,Mg)Si_2O_6$ pyroxenes: effect of the cation substitution on cell volume, Mineral. Mag. 81 (5) (2017) 1129–1139.
[6] V.M. Pogrebenkov, I.M.B. Sedel'nikovaflandl, V.I. Vereshchagin, Ceramic pigment with diopside and anorthite structures based on Wollastonite, Glass Ceram. 56 (1–2) (1999) 55–57.
[7] G. Durand, S. Vilminot, P. Rabu, A. Derory, J.P. Lambour, E. Ressouche Synthesis, Structure and magnetic properties of $CaMSi_2O_6$ (M = Co, Ni) compounds and their solid solutions, J. Solid State Chem. 124 (1996) 374–380.
[8] M.A. Tena, Rafael Mendoza, Camino Trobajo, José R. García, Santiago García-Granda, Green and blue materials for the ceramic industry from pink $MgCo_xNi_{1-x}SiO_4$ ($0 \leq x \leq 1$) solid solutions, Ceram. Int. 49 (2023) 12021–12033, https://doi.org/10.1016/j.ceramint.2022.12.052.
[9] S. Masse, P. Boch, Nicolas Vaissiere, Trapping of nickel and cobalt in $CaNiSi_2O_6$ and $CaCoSi_2O_6$ diopside-like phases in heat-treated cement, J. Eur. Ceram. Soc. 19 (1999) 93–98.
[10] M.A. Tena, Rafael mendoza, camino trobajo, santiago garcia-granda. Cobalt minimisation in violet $Co_3P_2O_8$ pigment, Materials 15 (1111) (2022) 1–14, https://doi.org/10.3390/ma15031111. https://www.mdpi.com/1996-1944/15/3/1111/pdf.
[11] M.A. Tena, Rafael Mendoza, Camino Trobajo, José R. García, Santiago Garcia-Granda, Ceramic pigments from $Co_xNi_{3-x}P_2O_8$ ($0 \leq x \leq 3$) solid solutions, Ceram. Int. 47 (21) (2021) 29888–29899, https://doi.org/10.1016/j.ceramint.2021.07.162.
[12] H.M. Rietveld, A profile refinement method for nuclear and magnetic structures, J. Appl. Crystallogr. 2 (1969) 65–71.
[13] J. Rodriguez-Carvajal (September 2018-ILL-JRC), Fullprof.2k Computer Program, Version 6.50, France.
[14] L. Chapon (Rutherford Appleton Laboratory, UK) and J. Rodriguez-Carvajal (Institut Laue Langevin, France) (August 2008). FPStudio Computer Program, Version 2.0..
[15] Inorganic Crystal Structure Database (ICSD web). Fachinformationszentrum (FIZ, Karlsruhe, Germany..
[16] Commission Internationale del'Eclairage (1978), Recommendations on Uniform Color Spaces, Color Difference Equations, Phychometrics Color Terms, Supplement No. 2 to CIE Publication No. 15 (E1-1.31), Bureau Central de la CIE, Paris, 1971.
[17] M. Tribaudino, L. Mantovani, F. Mezzadri, G. Calestani, G. Bromiley, The structure of P21/c $(Ca_{0.2}Co_{0.8})CoSi_2O_6$ pyroxene and the C2/c–$P2_1/c$ phase transition in natural and synthetic Ca–Mg–Fe^{2+} pyroxenes, Mineral. Mag. 82 (1) (2018) 211–228.
[18] R.D. Shannon, Acta Crystallogr. A32 (1976) 751.
[19] H. Azzi, I. Rekkab-Hammouraoui, L. Chérif-Aouali, A.C. Kchou-Braham, Mesoporous Co_3O_4 as a new catalyst for allylic oxidation of cyclohexene, Bull. Chem. React. Eng. Catal. 14 (1) (2019) 112–123.
[20] X. Liu, C.T. Prewitt, High-temperature X-ray diffraction study of Co_3O_4: transition from normal to disordered spinel, Phys. Chem. Miner. 17 (1990) 168–172.
[21] S. Khan, C. Wang, H. Lu, Y. Cao, Z. Mao, C. Yan, X. Wang, In-situ tracking of phase conversion reaction induced metal/metal oxides for efficient oxygen evolution, Sci. China Mater. 64 (2021) 362–373.
[22] H.W. Nesbitt, D. Legrand, G.M. Bancroft, Interpretation of Ni2p XPS spectra of Ni conductors and Ni insulators, Phys. Chem. Miner. 27 (2000) 357–366.
[23] M.A. Tena, R. Mendoza, C. Trobajo, J.R. García, S. García-Granda, $Co_2P_2O_7$–$Ni_2P_2O_7$ solid solutions: structural characterization and color, J. Am. Ceram. Soc. 102 (2019) 3695–3704, https://doi.org/10.1111/jace.16158.